Application of a Novel Multi-Principal Element Alloys for Solid-State Hydrogen Storage Enabling Room-Temperature Activation

Eugene Ahn[1]

Received March 22, 2026
Accepted July 10, 2026
Electronic access September 15, 2026

Hydrogen energy is interesting as a clean fuel for the future, while it also concerns regarding its safety problem being raised. Generally, gas hydrogen always keeps expensive high-pressure tanks, has a low energy density, and is able to potentially explosion situation. Liquid hydrogen also has a low safety and high cost to transport and store, requires cooling down below -253°C. Otherwise, the solid-state hydrogen stored by hydrogen storage alloy is stable and confirms the high energy density through maintaining it in metal lattice. However, conventional TiFe-based hydrogen storage alloys require high energy and temperature to active the hydrogen storage properties, also charge-discharge process have a high cost with low storage. In this study, the multi-principal element alloys (MPEAs) applied to hydrogen storage materials to overcome these limitation. MPEAs exhibit a simple solid-solution structure and excellent stability, as the entropy of mixing overcomes the enthalpy of mixing. MPEA powders were synthesized via mechanical alloying; their stable phases were verified through thermodynamic calculations, their microstructures were analyzed using X-ray diffraction and electron microscopy, and their hydrogen storage characteristics were measured at 10 atm and room temperature using the Sieverts method. The alloy exhibited an FCC structure and significant lattice distortion, enabling initial hydrogen activation without external heating and achieving a hydrogen storage capacity of 1.3 wt.%. These findings suggest that MPEAs have the potential to serve as next-generation hydrogen storage alloys in the hydrogen energy fields.

Keywords: Hydrogen Storage, Multi-Principal Element Alloys (MPEAs), Solid-State Reaction, Mechanical Alloying, Severe Lattice Distortion, Room-Temperature Activation, Hydrogenation

Introduction

Long-term instability of climate change, air pollution and fossil fuel supplies are accelerating the search for alternative energy systems. Among the many proposed solutions, hydrogen has been identified as a key energy carrier in a future low-carbon economy When hydrogen is used for a fuel cell or combusted with oxygen, water is produced instead of carbon dioxide. Due to this chemical property allows hydrogen to serve as attractive decarbonizing sectors that are difficult to direct electrification, heavy transportation, steel production, shipping and large-scale energy storage[1]. In addition, hydrogen can serve as an energy buffer: excess electricity generated from intermittent renewable energy sources such as wind or solar power can be converted into hydrogen and later reconverted into electricity when needed. So, hydrogen is not only considered simply as a fuel, but also as a bridge connecting renewable energy generation with a stable supply[2]. However, the characteristics of hydrogen indicate a major obstacle. Under room temperature and 1 atm, hydrogen is light gas with very low density. Thus, storage of hydrogen in a compact and safe form is challenging point. Generally, hydrogen is stored in three type states: compressed gas, liquid, and solid-state in metal-hydride with their own pros and cons[3].

Compressed hydrogen storage is well established technology and already applied in prototype fuel cell vehicles[4]. Hydrogen is stored in high pressure tanks typically $\sim$700 bars. However, the high-pressured gas requires tanks based on high mechanical properties with safety design and regular inspection. Although hydrogen gas is under high pressure, it contributes to low density compared to conventional fuels. Due to these limits driving range and increase the overall weight of the hydrogen storage system. Liquid hydrogen storage systems improve volumetric density by cooling hydrogen below its boiling point of -253°C[5]. The liquid state hydrogen is higher density than compressed gas, but liquefaction requires significant energy that is larger than stored energy. Also, cryogenic conditions of hydrogen require advanced insulation technology, and it is evaporating and losing that occur during long-term storage[6]. These limitations occurred attention of solid-state hydrogen storage such as the metal-hydride storage systems storing hydrogen atoms in interstitial sites of metal are efficient and safe. This method densifies hydrogen under normal conditions and reduces risk compared to other methods. Thus, hydrogen storage alloys are attractive materi-

[1] *Seoul International School, Republic of Korea*

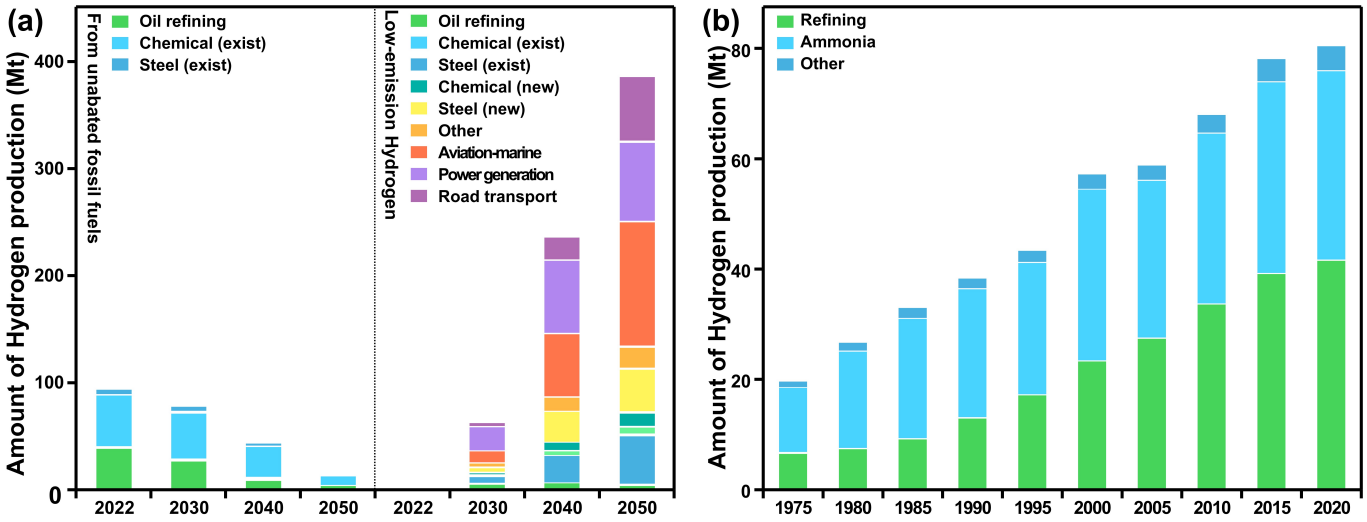

Figure. 1 (a) Global hydrogen demand based on recent international energy outlook reports (IEA) [1], (b) Historical global demand for pure hydrogen from 1975 to 2020 [2].

als as candidates for compact and safer hydrogen energy and transport[7].

Figure 1(a)[8] shows the global hydrogen demand based on recent international energy outlook reports. The graph shows continuously increasing hydrogen integrated into transportation, industry, and power generation. The demand increase is significant, indicating national commitments to carbon neutrality and the expansion of hydrogen-based technologies. Figure 1(b)[9] indicated historical data on global demand for pure hydrogen. In Figure 1(b), combined with the future projections in Figure 1(a), suggests that hydrogen is expected to play a much larger role in the global energy landscape. Improvements in hydrogen storage materials have become increasingly important[10].

Numerous intermetallic hydrogen-storage alloys have been developed and studied such as $LaNi_5$, TiFe, ZrNi, $TiCr_2$, and Mg_2Ni among the most widely investigated systems with the formation of hydrides[11]. TiFe-based alloys are attended because they are composed of cheap elements and exhibit moderate hydrogen storage capacity as $\sim$1.0 wt.% at room temperature. These alloys show cycling stability that conventional hydrogen storage alloys still encounter numerous substantial limits. However, one of the most important issues of hydrogen storage materials is first-cycle activation. TiFe-based alloys cannot hydrogen absorption begin immediately under room temperature. Elevated temperature or high hydrogen pressure is usually required to initiate hydrogen activation. This process increases system complexity and energy consumption. Mg-based alloys provide a higher capacity to density; they require even higher temperatures for activation and exhibit slow hydrogen absorption–desorption kinetics. Alloys containing rare-earth elements can achieve favorable hydrogenation behavior but introduce concerns related to cost and resource availability[12]. These conventional storage systems involve different thermodynamic parameters. So, an alloy design that combines structural stability with lattice distortion and defect-assisted hydrogen transport is needed for milder activation behavior[11,12].

Thermodynamic balance is also a challenge that needs to be addressed. If the enthalpy of hydride formation is too negative, hydrogen becomes difficult to release. Compositional design should be confirmed to achieve high storage capacity and repeatability under lower temperature and pressure. These limitations suggest that conventional binary and ternary intermetallic systems may not fully satisfy the requirements of next-generation hydrogen storage. So, new alloy design concepts that move beyond conventional composition strategies are being explored. Multi-principal element alloys are combined in similar atomic fractions to introduce configurational entropy stabilization and lattice distortion effects. Such compositional complexity can influence hydrogen diffusion pathways and reduce activation barriers remains an open question and is still under active investigation[13].

Multi-principal element alloys (MPEAs) have recently emerged as an alloy-design strategy that departs from conventional binary and ternary intermetallic systems. Conventional hydrogen-storage alloys are typically based on classical AB-, AB2-, and AB5- type structures, in which a single principal element dominates the composition and minor substitutions are used to tune thermodynamic properties. MPEA, by contrast, makes a complexity of compositions by combining several metallic components, which causes a whole change

of phase stability and structure properties. This approach increases configurational entropy; Otherwise, it can stabilize disordered solid solution phases even if several intermetallic structures were formed. As the composed elements have different characters—such as atomic radios, combine tendency, electronegativities—structures show clear distortion and local atomic displacement. In the case of hydrogen storage materials, these features are not coincidental; hydrogen absorption depends on the availability of interstitial sites, lattice distortions, and the hydride formation enthalpy. The distorted lattice which has various chemical conditions, can affect hydrogen storage behavior (Figure 2)[14].

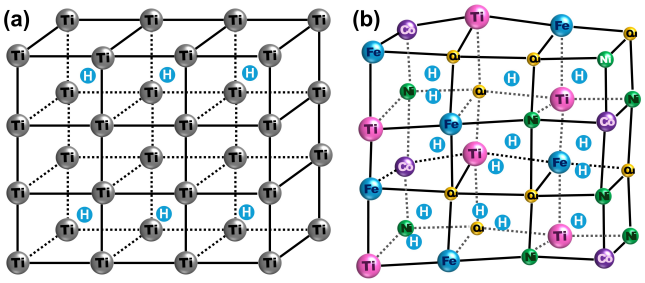

Figure. 2 Structural schematic illustrating hydrogen storage in solid-state alloys: (a) Conventional alloy with uniform lattice, (b) Multi-principal element alloy (MPEA) exhibiting lattice distortion and diverse interstitial sites after hydrogen incorporation.

The attention to the MPEA for hydrogen storage has increased, but it is still at an early stage compared to the research of TiFe- or $LaNi_5$- based materials. Initial research mainly focuses on the structural and mechanical properties of multi-component alloys, while the next stage focuses on the hydrogen absorption behavior. Refractory elements-based MPEA shows the capability of hydride formation, some cases report that the hydrogen occupation occurred at many interstitial sites because of the severe lattice distortion. Although the study about the multi-components system including Mg was animated on the high theoretical weight capacity, usually high temperature is needed in real activation. Reported hydrogen storage capacity is highly dependent on the phases, chemical alloying compositions, and manufacturing processes. Some systems almost form FCC or BCC solid solutions, whereas others contain Laves phase or ordered intermetallic phase that affect hydride formation pathway. These results suggested that the control of the phase stability and the microstructure are still important for availability of hydrogen absorption of the MPEA. However, the role of MPEA structure at the first hydrogen activation cycle is not clearly investigated yet. Most studies are focused on hydride stability of total storage capacity, but the studies whether the lattice distortion and localized chemical complexity can turn down activation barriers in mild conditions are relatively little. Though, the research about the room temperature activation of the hydrogen storage alloy based on the MPEA still remains an important research gap.

Almost hydrogen absorption-MPEA studies were conducted by solidification after the arc melting process, which forms bulk alloys with relatively rough structures. Meanwhile, Mechanical Alloying (MA) provides different processing methods. High energy ball milling promotes repeated fracture and cold welding of powder particles, which facilitate the micro powder size, increased chemical homogeneity, and controlled phase transformation. In the hydrogen storage research, the MA was used to activate the TiFe- based system, because it can introduce stacking faults and increase surface area over a long duration. Therefore, if MA is introduced in MPEA, it can achieve complexity of formation by designing multi-component systems and microstructure refinement because of severe plastic deformation. Reactive milling under hydrogen conditions was attempted on several multi-component systems, which formed hydrides directly during the process; the results for capacity and reversibility are quite different among the systems. Certain Mg-containing MPEA shows proper hydrogen absorptions, whereas others show limited interaction with hydrogen in particular phases. Those mixed results suggest that the increasing complexity of formation does not always guarantee increased hydrogen storage capacity; instead, interaction among phase constitutions, lattice distortions, and thermodynamics should be considered[15].

The multi-component alloys based on Fe, Co, and Ni are used to stabilize solid solutions easily, and the introduction of Ti and Cu can affect oxidation behavior and lattice strain. Therefore, CoCuFeNiTi, which derived from the TiFe-based materials, was selected for the MPEA system; in this system, Ti and Fe serve as hydrogen storage base, Co and Ni stabilize multi-component FCC-based structure, and Cu modifies the local surface condition and lattice strain during initial hydrogen interaction. TiFe material is one of the most studied materials because it has a proper capacity at room temperature and its cost is relatively low. Nevertheless, the TiFe-based system still needs a caution at the activation process, which often involves high temperature or high hydrogen pressure during the first cycle. Surface oxidation layers and the kinetic barrier to hydrogen diffusion limit direct absorption at room temperature. Previous studies on TiFe-based hydrogen storage materials were conducted at high temperature of 300°C and under high pressure within the tens of atmosphere range. Thus, achieving hydrogen activation under milder conditions remains an important goal for solid-state hydrogen storage materials. If a multi-component approach can stabilize lattice characteristics to decrease such barriers, it could open the path to achieving useful activation behavior without rare-earth elements or extreme processing conditions[16].

In this study, CoCuFeNiTi multi-component alloys were

produced by mechanical alloying, and whether hydrogen absorption under practical conditions can be improved by combining compositional complexity with microstructure refinement was investigated. This study not only focuses on increasing storage capacity but also treats the issue of first cycle activation at room temperature, which remains an important limitation of conventional hydrogen storage systems. Phase stability is measured and thermodynamic parameters are calculated, and the results are used to establish phase evolution and lattice constant. After that hydrogen absorption behavior was tested at room temperature to evaluate activation performance. In this research, we related structure features to hydrogen absorption to investigate how the MPEA design strategy affects activation behavior and whether it can provide a practical way to overcome the continuous activation limitations observed in conventional hydrogen storage alloys.

Results

Thermodynamic calculation of CoCuFeNiTi MPEA

Before doing experimental analysis, several thermodynamic and geometric parameters were calculated to evaluate whether CoCuFeNiTi (MPEA) alloy can satisfy the generally accepted standard for solid solution formation. In multicomponent alloys, phase stability can be affected not only single factors but also many factors together, including configurational entropy (ΔS_{conf}), mixing enthalpy (ΔH_{mix}), atomic size difference (δ), and electronic structure. In these parameters shown whether alloys can form a stable solid solution or multiphase structure. They should be considered as guidelines for phase stability and lattice distortion, not as direct guidelines for hydrogen storage capacity or activation behavior Therefore, we used the calculated parameters only to discuss phase stability and lattice distortion, and the hydrogen absorption was evaluated separately through hydrogen test. Table 1 shows MPEA's calculated thermodynamic parameters[17].

To quantitatively assess phase stability in the CoCuFeNiTi MPEA, several thermodynamic parameters used for MPEA systems were calculated. These parameters are applied in evaluating whether a composition is likely to form a stable solid solution or to decompose into multiple intermetallic phases.

The configurational entropy (ΔS_{conf}) was calculated using the standard expression:

$$\Delta S_{\text{conf}} = -R\sum_i c_i \ln c_i \tag{1}$$

where R is the gas constant (8.314 J mol^{-1} K^{-1}) and Ci represents the atomic fraction of each constituent element. For the present alloy, ΔS_{conf} was calculated to be 13.07 J mol^{-1} K^{-1} that lies within the range associated with entropy-stabilized multicomponent alloys. A high configurational entropy indicates a significant degree of chemical disorder, which thermodynamically favors the stabilization of disordered solid-solution phases over ordered intermetallic compounds.

The mixing enthalpy (ΔH_{mix}), which reflects pairwise atomic interactions between different elements, was determined using:

$$\Delta H_{\text{mix}} = 4\sum_{i<j} H_{ij} c_i c_j \tag{2}$$

where H_{ij} denotes the binary mixing enthalpy between elements i and j. The calculated ΔH_{mix} value of -5.51 kJmol^{-1} suggests moderately negative atomic interactions. Instead, it implies that while solid-solution phases may be stabilized, secondary intermetallic phases cannot be excluded[18].

To evaluate the relative influence of entropy and enthalpy, the Ω parameter was calculated:

$$\Omega = \frac{T_m \Delta S_{\text{conf}}}{|\Delta H_{\text{mix}}|} \tag{3}$$

where T_m is the average melting temperature of the alloy, calculated by the rule of mixtures from the melting temperatures of Ti, Fe, Co, Ni, and Cu. For the present composition, Tm was calculated to be approximately 1676 K. The resulting Ω value of 3.98 is significantly greater than the commonly referenced stability criterion ($\Omega > 1$). From a thermodynamic perspective, the entropy contribution is sufficiently strong to compete with the enthalpy term and promote solid-solution stabilization.

Atomic size mismatch (δ), which quantifies lattice distortion arising from differences in atomic radii, was calculated as:

$$\delta = \sqrt{\sum_i c_i \left(1 - \frac{r_i}{\bar{r}}\right)^2} \times 100 \tag{4}$$

where r_i is the atomic radius of element i and $\bar{r}$ is the average atomic radius. The calculated δ value of 6.76% indicates

Table 1 Calculated thermodynamic parameters of the CoCuFeNiTi MPEAs

Composition	ΔS_{conf}	ΔH_{mix}	Ω	δ	VEC_{mix}	$\Delta\chi$
TiFeCoNiCu	13.07 J mol^{-1} K^{-1}	-5.51 kJ mol^{-1}	5.85	6.76%	8.79	0.173

substantial lattice distortion. This distortion is relevant for hydrogen-storage materials because it can influence the distribution of interstitial sites available for hydrogen occupation.

The valence electron concentration (VEC), which is often used to predict preferred crystal structure, was determined by:

$$VEC_{\text{mix}} = \sum_i c_i VEC_i \tag{5}$$

The calculated VEC_{mix} value of 8.79 falls within the range typically associated with FCC phase stability. This prediction is consistent with the FCC-based phases later identified through X-ray diffraction analysis[19].

The electronegativity difference ($\Delta\chi$) was calculated using:

$$\Delta\chi = \sqrt{\sum_i c_i \left(\chi_i - \sum c_j \bar{\chi}_j\right)^2} \tag{6}$$

where χ_i represents the electronegativity of each element. The obtained $\Delta\chi$ value of 0.173 suggests moderate chemical non-uniformity within the alloy. Such non-uniformity can promote local variations in bonding character and may facilitate the formation of minor secondary phases, including Laves-type structures[20].

Phase transformation of CoCuFeNiTi MPEA

XRD was used to analyze phase evolution of CoCuFeNiTi MPEA while mechanical alloying, and the results are shown in Figure 3. The diffraction patterns show the change while milling time increases. After 5 h milling, alloys do not show single phase. Instead, TiFe rich, NiCu rich and clear C14 Laves phase diffraction peaks were observed. Also, weak NiTi ordering peaks are observed in the pattern. In this step, the powder undergoes repeated collisions and cold welding, but atomic diffusion was still unstable. Coexistence of several intermetallic peaks mean the segregation of powder, because homogenization limits. When the milling time became 15 h, diffraction profile showed a noticeable change. The FCC1 peak became stronger, while intermetallic peaks decreased and disappeared. Continuous high-energy milling improved atomic mixing that mechanical alloying repeatedly breaks and welds the powder to reduce the diffusion distance and cause the elements to penetrate each other. The separated TiFe rich and NiCu regions become to dissolve into continuous solid solution matrix. Decreasing and disappearing intermetallic peaks suggest that ordering broke and the system became chemically disordered[21].

The diffraction pattern showed a change after 45 h milling. Now the alloy becomes two FCC phases, called FCC1 and FCC2, with only weak C14 Laves peak remaining. The two FCC peaks, not a single peak, indicate small compositional differences that remained in the structure, because of local chemical distribution. Furthermore, the overall pattern became simpler compared with initial condition. The intermetallic compounds were no longer clear at 5 h milling. It means long time of mechanical deformation made these ordered phases unstable and enter their atoms into FCC matrix.

Fine peak shifts become clear during milling. Shifting into lower angles of FCC2 reflection means increase of the lattice parameter, while the FCC1 and Laves peak shifts into higher angles. This opposite shifting means local composition rearrangement between the two FCC phases. Change of Lattice parameter match with the difference in atomic size of Co, Cu,

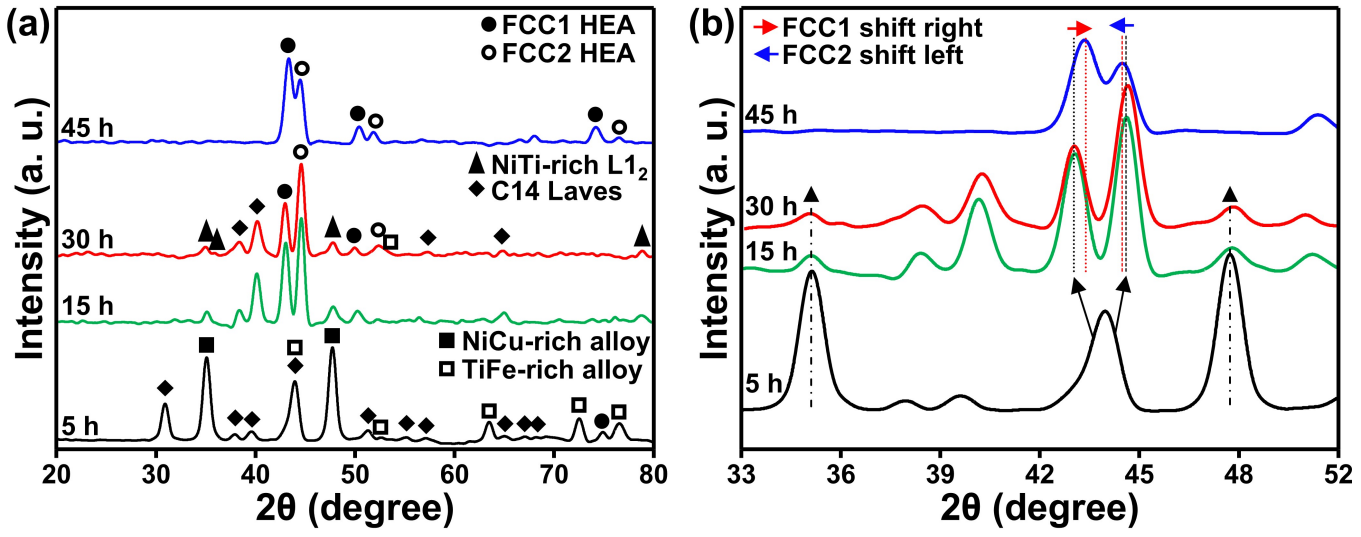

Figure. 3 X-ray diffraction pattens of CoCuFeNiTi MPEA (a) after mechanical alloying at different milling time, (b) enlarged view of main diffraction peaks of (a).

Fe, Ni, Ti. A calculated atomic size mismatch ($\delta = 6.76\%$) can be expected to be a measurable lattice distortion. Thus, the observed peak shifts are related to strain accumulation and internal lattice change, instead of simple phase change. The value of calculated electronegativity ($\Delta\chi = 0.173$) can be evident for short range chemical ununiform, and this can contribute to small amount of topologically close packed structures. Crystallite size and lattice strain were calculated with the Scherrer equation. Small increase in crystallite size occurred from 15 h to 30 h because of cold welding and agglomeration. However, at 45 h, severe plastic deformation and fracture reduced the crystallite size again. This result means particle breaking of alloys were more dominant than particle growth. Simultaneously, milling time can cause higher lattice strain, reflecting dislocation and accumulation of internal defects. Calculated dislocation density was shown, which means the increase of disordering during milling[22].

Microstructural evolution and elemental distribution

Figure 4 showed representative SEM images of difference of powder morphology during mechanical alloying. Clear differences observed as the milling time from 5 h to 45 h.

After 5 h milling, agglomerated irregular powder particles were observed. The coexist presence of large fragments and fine debris shows cold welding and fracture were both working but not reached stable state. Rough and mechanically deformed surfaces were observed because of repeated impact during high energy milling. At 15 and 30 h, broadening of the overall particle size observed. Agglomerate powder remained, but smaller particles became more superior in the matrix. At this point, the competition of cold welding and particle fracture becomes more clearly observed. Some particles can grow with welding temporarily while other particles break down. This kind of dynamic balance easily occurs during mechanical alloying of multicomponent.

After 45 h milling, the powder morphology clearly changed. Particle distribution becomes more uniform and larger agglomerates become less dominant. Most particles become finer and more dispersed. This refinement consists of severe plastic deformation and fracture after long time of milling process. The large number of defects during milling considered improved homogenization and change of the internal structure[23].

Figure 4(e) presents the EDS mapping for examine the elemental distribution. The results showed that Co, Cu, Fe, Ni, Ti were distributed without any clear segregation. At observed scale, no element was limited to a separate region, showing that long milling can successfully promote chemical mixing. This homogeneity is different from the early XRD structured results, that showed separate TiFe rich and NiCu rich phase. After 45 h milling, these chemically separated regions were re-

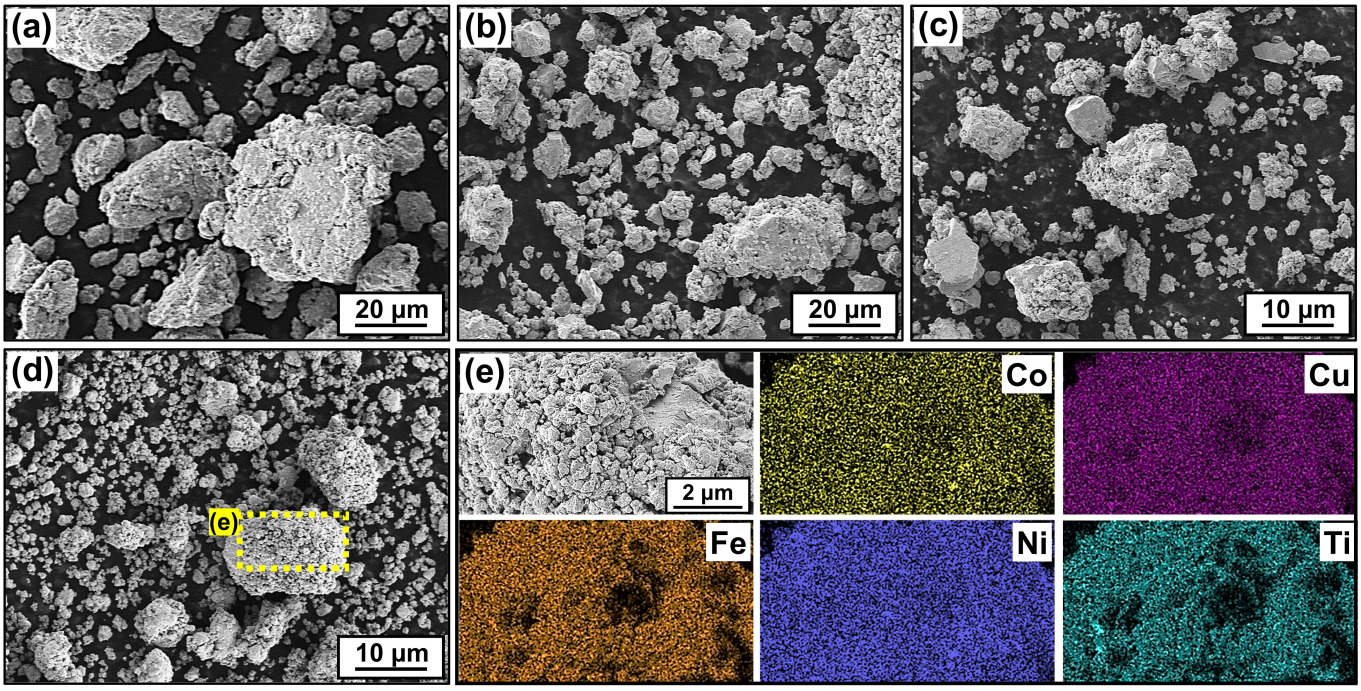

Figure. 4 SEM results of CoCuFeNiTi MPEA powders with increasing milling time: (a) 5 h, (b) 15 h, (c) 30 h, and (d) 45 h. (e) Corresponding EDS elemental maps of the 45 h milled powder, illustrating the spatial distribution of Co, Cu, Fe, Ni, and Ti.

duced. Instead of clear TiFe rich region, two FCC regions correspond to FCC1 and FCC2 in XRD results, consist of main structure. Small amount of Laves phase remained. Clear decrease of composition boundaries show that initial intermetallic phase gradually dissolved into FCC matrix. The compositions measured in 5 and 45 h milling were similar to nominal compositions. It means, no significant element loss occurred during milling[24].

Particle size analysis of CoCuFeNiTi MPEA

The particle size analysis results for CoCuFeNiTi MPEA powders are summarized in Figure 5. Distribution curves indicate clear changes while increasing milling time. This shows the competition mechanisms during mechanical alloying.

In the case of 5 hour milling powder, the powder showed a wide particle size distribution with large deviation. The particle size distributes nearly 100 μm. This shows the coexistence of coarse agglomerates and fine particles. In this step, repeated high energy impacts rapidly break the powders. And cold-welding leads to sticking between new surfaces. Significant deviation in particle size occurred because dynamic balance of two systems did not reach yet. The average particle size increased when the milling time to 15 h. This means cold welding momentarily stronger than fracture. During the middle step of milling, plastically deformed particles repeatedly fracture and attach to large agglomerates. The mechanical energy input could be enough to deform particles. But not enough to break the welded particle continuously. As a result, particle growth observed despite the fracture occurred continued.

When the milling continued to 45 h, this trend revered. The average particle size became smaller and distribution became sharp. After long deformation, strain accumulated inside the particles. Work hardening and heavy defects reduce the ductility, while welded agglomerates gradually become more brittle. With continuous fracture loading, these brittle particles broke more easily than welded. Therefore, fracturing became the dominant mechanism instead of cold welding. As a result, the powder showed more fine and uniform size distribution[25].

Thermal stability of CoCuFeNiTi MPEA

Figure 6 shows the results of differential thermal analysis (DTA) and thermogravimetric analysis (TGA) of mechanically alloyed CoCuFeNiTi MPEA powder. Figure 6(a) shows the DTA result, and Figure 6(b) shows the related mass changes from TGA.

Thermal phenomenon observed between 200 and 280 °C in DTA curve in Figure 6(a). Peaks indicated 200 °C, 237 °C, 242 °C, 278 °C depending on the milling condition. The powders used for DTA/TGA were not considered to be hydrogen desorption result, because the powders were not hydrogenated. DTA/TGA peaks were not considered to result in hydrogen desorption, because the powders were not hydrogenated before test. Instead, these peaks were considered thermal reaction, including structural relaxation, defect recovery or reactions related to metastable phases formed during milling. When milling time increases, the reaction temperature shift decreases and range becomes wider. This means long time of mechanical alloying produced a wider range of defect state and atomic environment.

Figure 6(b) shows the TGA curves of the relative change of

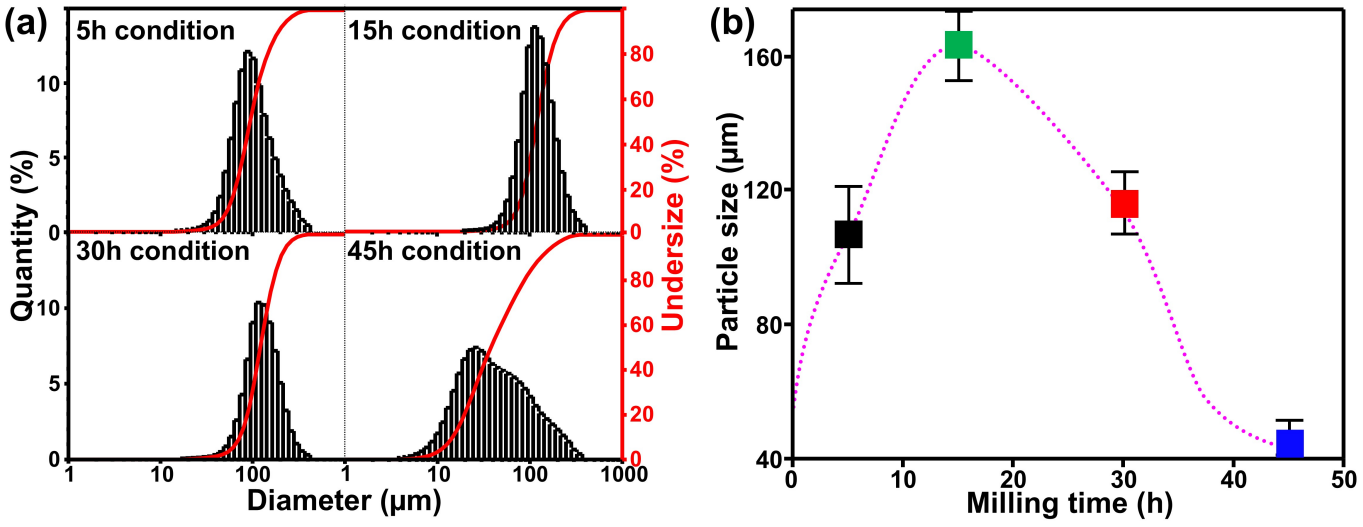

Figure. 5 (a) Particle size distribution curves of CoCuFeNiTi MPEA powders after 5 h, 15 h, 30 h, and 45 h of mechanical alloying. (b) Variation in average particle size with corresponding standard deviation.

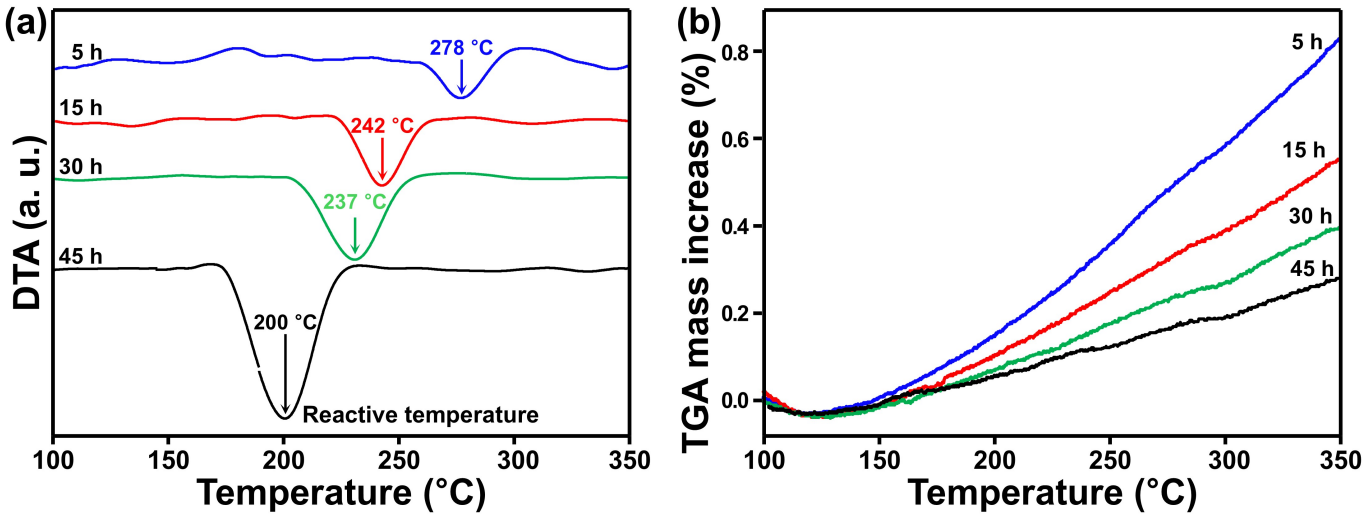

Figure. 6 Thermal analysis results of mechanically alloyed CoCuFeNiTi MPEA powders: (a) Differential thermal analysis (DTA) curves, (b) Thermogravimetric analysis (TGA) curves.

mass during heating. Because Ar gas was used, the change of mass reflects the thermal stability of mechanical alloying powder and resistance to oxidation mass increase. The mass increase small, this means the CoCuFeNiTi MPEA powders remained relatively stable during heating conditions. Mass gain decrease was found after long time milling. This means that improved chemical mixing and FCC based solid solution formation contributed much more thermal stability. Therefore, the DTA/TGA results were used for the discussion of thermal reaction and oxidation stability rather than hydrogen absorption and desorption. Mechanical alloying can produce fine powders with high specific surface area and increase defect density, making powders reactivity. Therefore, small changes of slope at high temperature can contribute to surface oxidation or structural rearrangement during heating. Higher surface activity corresponds to the smaller particle size analyzed in microstructure[26].

Specific surface area of CoCuFeNiTi MPEA

The specific surface area of the mechanically alloyed CoCuFeNiTi MPEA powders was investigated using Brunauer–Emmett–Teller (BET), and the results are shown in figure 7.

As the milling time increased, the surface area gradually increased. The measured value increased from 0.0604 ± 0.0009 m^2g^{-1} after 5 h of milling to $0.0972 \pm m^2g^{-1}$ after 45 h. The absolute values were relatively small; however, the tendency was consistent and reproducible. At the relatively low pressure ($p/p_0 < 0.3$), nitrogen adsorption-desorption isotherms did not present clear adsorption, while did not exhibit meaningful hysteresis Roop between adsorption-desorption branches. The absence of clear hysteresis Roop suggests that there is no connection between mesopore networks in the powder whereas adsorption behavior was mainly caused by surface exposure. In other words, the increase of BET surface is not the result of pore, but the particle refinement and surface roughening during mechanical alloying[27].

These interpretations correspond to the particle size results. Although rapid fracture produces fine fragments at the earlier milling stage, the agglomeration induced larger effective

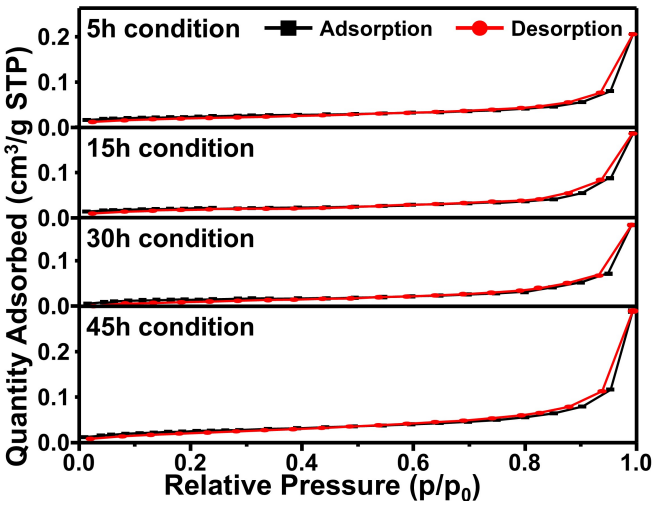

Figure. 7 Specific surface area of CoCuFeNiTi MPEA powders measured by BET analysis under nitrogen atmosphere as a function of mechanical alloying time.

size as the cold welding became dominant temporarily. As the milling proceeds, accumulated strain and work hardening reduces ductility, and agglomerates fractured more easily. As the milling time increases, decreased particle size increases available surface area. The parallel variation of PSA and BET results supports these mechanisms[28].

Hydrogenation activation of CoCuFeNiTi MPEA

Hydrogen absorption of CoCuFeNiTi MPEA was investigated using Sieverts' apparatus at room temperature under initial hydrogen pressure of 10 atm.

The recorded pressure during the activation process and subsequent first hydrogenation cycle is shown in figure 8(a). Immediately after hydrogen charging into the reactor, the system entered the labeled "activation cycle" stage. In this stage, the pressure was not constantly maintained. Instead, the pressure continuously dropped to approximately 0.98 atm for the first 5 min. This suggests that the absorption of hydrogen was started without heating or long delay. This initial drop of pressure corresponds to hydrogen dissociation on the particle surface and absorption on the near surface. The measurable absorption at the initial stage suggests that although the possibility of oxide, mechanically alloyed surfaces allowed hydrogen penetration under pressure with sufficient surface activation. After this first decrease of pressure, the system reached a temporal equilibrium state with stabilized pressure. At this point, hydrogen was recharged to the system to increase the pressure 10 atm. This depressurization corresponds to transition from activation stage to first hydrogenation cycle. Once the pressure was reset, alloy absorbed hydrogen, and second pressure deep until approximately 1.03 atm for before the 3 min. This magnitude of drop is slightly larger and occurs more rapidly than the activation stage. These differences suggest that alloy reacted more sensitively after the initial activation stage. The activation stage may disrupt the surface barrier and connect the diffusion path into the lattice which enables faster hydrogen absorption during the first cycle. After this rapid absorption, pressure gradually decreased until a new equilibrium state[29]. Figure 8(b) shows pressure variations during the first hydrogenation cycle except for the activation stage. The time axis expressed in minute and presented substantial absorption dynamics after activation. Curves showed rapid initial slope during the initial stage of the first cycle, which indicates rapid hydrogen absorption. This behavior of the first stage is generally related to surface adsorption and short range diffusion into a severely distorted lattice. The slope gradually decreased as time progressed, which indicates the hydrogen transport was controlled diffusion into the matrix. Pressures continually dropped until stable equilibrium started at approximately 120 min, which means about 1.3 wt.% H_2 hydrogen storage[30].

Combine the two-stage pressure response shown in figure 8(a) with continuous absorption profile shown in figure 8(b), providing insights of activation mechanisms. Conventional TiFe alloy requires high temperatures (300–400 °C) or repetitive cycling for establishing stable hydrogen absorption. In contrast, the present MPEA proceeds stable hydrogen absorption under appropriate pressure and is entirely activated at room temperature. The observed room temperature activation behavior can relate to refined particles, high defect density induced by mechanical alloying and dual fcc-based phase. Since the diffusion coefficient and hydrogen site occupancy are not measured, the role of lattice distortion should be con-

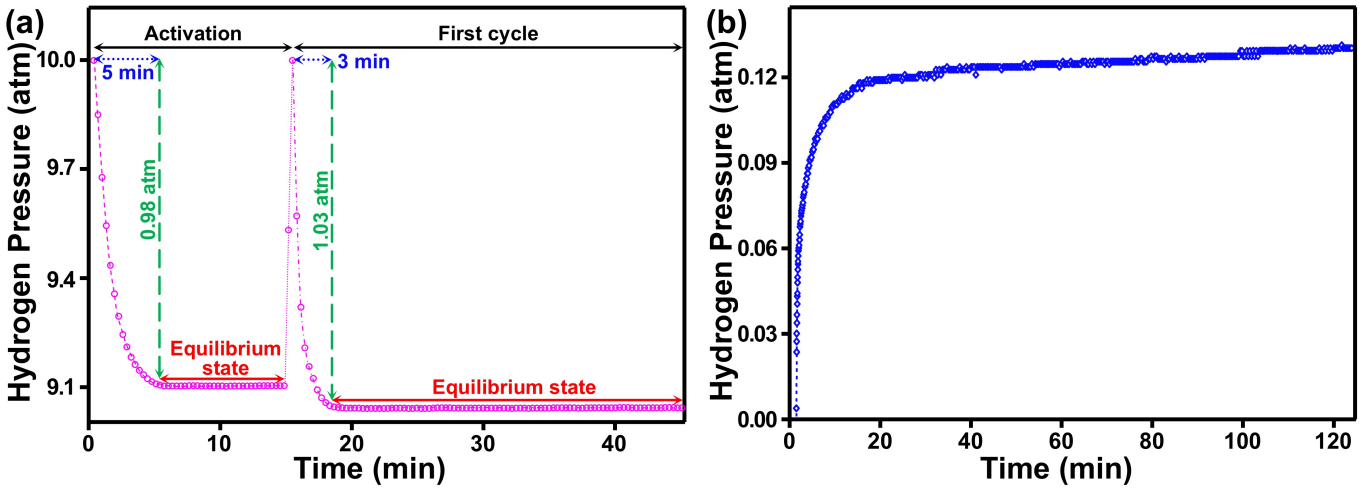

Figure. 8 Hydrogenation behavior of CoCuFeNiTi MPEA powders mechanically alloyed for 45 h and subsequently exposed to hydrogen at 30 °C under an applied pressure of 10 atm. (a) Pressure profile during the activation stage followed by re-pressurization and the first hydrogenation cycle. (b) Hydrogen pressure changes with time during the first hydrogenation cycle.

sidered as a possible interpretation. Pressure response indicates hydrogen absorption during the first cycle at room temperature; however detailed activation mechanisms should be verified through measurement[31].

Discussion

Room temperature hydrogen storage responses present the most significant results. Hydrogen absorption initiated at 30 °C under 10 atm without pre-treatment and achieved 1.3 wt.% H_2 storage during the first cycle. Previous studies about TiFe- or MPEA-based hydrogen storage alloys usually carried out activation treated over than 300 °C to induce stable absorption and applied hydrogen pressure over than 50 atm. Therefore, although the presented storage should be interpreted not as reversible storage capacity but absorption mass during the first cycle, these results have value that can achieve activation during the first cycle under easy conditions. Conventional FCC-based hydrogen storage alloys usually limit the gravimetric capacity to about 1.0 wt.% under similar comparable conditions. In contrast, the present study shows superior storage capacity under room temperature conditions[2]. According to XRD, SEM-EDS and particle size analysis, alloy maintains the FCC-based MPEA which includes measurable lattice distortion and refined particle size. These properties may promote hydrogen absorption by providing short diffusion paths and local insertion sites[31].

Thermodynamic calculations indicate that alloy satisfies the standard of multi-component system stability. High configuration entropy and Ω parameter suggest that solid solution phase can be stabilized, while appropriate mixing enthalpy and difference of atomic radius predicted lattice distortion can occur[17]. MPEA maintained a structural stability local stress field, rather than an unstable multi-phase[18]. XRD[19] and microstructure results show that longtime mechanical alloying transformed separated intermetallic compounds at initial state to FCC-based solid solution[14]. Diffraction peak shifting and broadening indicates not the chemical instability but accumulated strain. SEM-EDS map shows gradual homogenization and grain refinement as the milling time increased. In other words, microstructural evolution indicates not the random mixing but stabilization of a distorted FCC matrix by featuring ordered compounds. This distortion may affect distribution of insertion sites which affect the hydride energy dynamics[20].

Particle shape and size results correspond to this structural deformation. Fracture-cold welding-refracture step caused refinements during longtime milling[23]. BET results show that surface area systemically increased, which was caused by decrease of particle size rather than pore. As surface exposure increased, the hydrogen diffusion range decreased, and surface reactivity increased. Therefore, lattice distortion and surface refinement both contribute to improving the hydrogen absorption dynamics[22]. Thermal analysis shows that reaction temperature was slightly decreased and reaction range was enlarged as the milling time increased. These results were not interpreted as hydrogen desorption because non-hydrogenation powder was used for DTA/TGA analysis. Instead, enlarged reaction range is interpreted as evidence of structural relaxation or defect-based reaction which was induced by mechanical alloying. Results of insignificant mass change shown in TGA suggest that mechanical alloyed CoCuFeNiTi powder maintained excellent thermal and oxidation stability. In other words, this alloy possesses both thermal stability and structural complexity[30].

Regarding hydrogenation, presented performance corresponds to the strategy of alloy design. A stable MPEA matrix was maintained, while lattice distortion provided additional hydrogen pathways. Activation phenomenon under relatively low pressure at room temperature suggests that the dynamic barrier which is reported in conventional FCC-based hydrogen storage alloys has decreased. Therefore, these performance improvements can be discussed that FCC-based phase, lattice distortion, defect accumulation and refined powder affect complexly rather than single mechanism[12].

The present study presents that MPEA design can improve room temperature hydrogen storage performance without hindering structural stability. The hydrogen storage properties can be controlled in a favorable direction by element complexity and controlled mechanical processing, without substitution to rare earth elements or extreme thermal activation[13].

Methods

Ti, Fe, Co, Ni, and Cu powders (purity: >99%) were used as starting materials. Mechanical alloying was carried out using a planetary ball mill (RETSCH PM-400MA, Germany) with 500 mL SUS304 jar and 20 mm diameter SUS304 balls and ball-to-powder ratio of 20:1. The milling energy was ∼21 gravity energy. Milling was performed under Ar 100% atmosphere at 300 rpm for 5, 15, 30, and 45 h. Phase evolution of as-milled powders was measured by X-ray diffraction (Rigaku D/MAX-Ultima III, Cu Kα radiation). Microstructure and elemental distribution were observed via FE-SEM with EDS (JEOL JSM-7500F). Particle size of powder milled 5 h, 15 h, 30 h, and 45 h was measured by PSA (Horiba LA-350), with five times to confirm accuracy. Thermal behavior was evaluated using differential thermal analysis and thermogravimetric analysis (Pyris Diamond, Perkin Elmer, Germany). The measurement was performed using non-hydrogenated powder with a sample mass of 38.31 mg under Ar flow at 50 sccm, and the heating rate was fixed at 10 °C/min. Specific surface area was determined using nitrogen adsorption–desorption isotherms based on the Brunauer–Emmett–Teller method (Mi-

cromeritics ASAP-2020). Hydrogenation behavior was evaluated using Sieverts-type utilities within high-purity (99.99%) hydrogen gas at room temperature under 10 atm. The activation of hydrogen storage for this matarials were measured through pressure change with time change.

References

1 J. A. Turner. Sustainable hydrogen production. Science 305, 972–974 (2004) .

2 L. Schlapbach, A. Züttel. Hydrogen-storage materials for mobile applications. Nature 414, 353–358 (2001) .

3 International Energy Agency. Global hydrogen review 2023. https://www.iea.org/reports/global-hydrogen-review-2023 (2023).

4 I. Sreedhar, K. M. Kamani, B. M. Kamani, B. M. Reddy, A. Venugopal. A bird's eye view on process and engineering aspects of hydrogen storage. Renewable and Sustainable Energy Reviews 91, 838–860 (2018) .

5 M. Hirscher. Handbook of hydrogen storage: new materials for future energy storage. Wiley-VCH (2010) .

6 M. Paskevicius, L. H. Jepsen, P. Schouwink, R. Cerny, D. B. Ravnsbæk, Y. Filinchuk, M. Dornheim, F. Besenbacher, T. R. Jensen. Metal borohydrides and derivatives – synthesis, structure and properties. Chemical Society Reviews 46, 1565–1634 (2017) .

7 U.S. Department of Energy. Hydrogen storage https://www.energy.gov/eere/fuelcells/hydrogen-storage (2023).

8 IEA Paris. Global hydrogen demand in the net zero scenario, 2022–2050. IEA. https://www.iea.org/data-and-statistics/charts/global-hydrogen-demand-in-the-net-zero-scenario-2022-2050 (2023).

9 IEA Paris. Global demand for pure hydrogen, 1975–2020. IEA. https://www.iea.org/data-and-statistics/charts/global-demand-for-pure-hydrogen-1975-2020 (2021).

10 IEA Paris. Progress in low-emissions hydrogen production, 2020–2030. IEA. https://www.iea.org/data-and-statistics/charts/progress-in-low-emissions-hydrogen-production-2020-2030 (2025).

11 U.S. Department of Energy. Hydrogen storage – how hydrogen storage works. U.S. Department of Energy. https://www.energy.gov/eere/fuelcells/hydrogen-storage (2019).

12 F. Marques, M. Balcerzak, F. Winkelmann, G. Zepon, M. Felderhoff. Review and outlook on high-entropy alloys for hydrogen storage. Energy Environmental Science 14, 5191–5227 (2021).

13 S. K. Dewangan, M. Mohan, V. Kumar, A. Sharma, B. Ahn. A comprehensive review of the prospects for future hydrogen storage in materials-application and outstanding issues. International Journal of Energy Research 46, 16150–16177 (2022).

14 B. Cantor, I. T. H. Chang, P. Knight, A. J. B. Vincent. Microstructural development in equiatomic multicomponent alloys. Materials Science Engineering A 375–377, 213–218 (2004).

15 A. Sharma, H. Lee, B. Ahn. Effect of additive elements (x = Cr, Mn, Zn, Sn) on the phase evolution and thermodynamic complexity of AlCuSiFe-x high entropy alloys fabricated via powder metallurgy. Metals and Materials International 28, 2216–2224 (2022).

16 H. Lee, S. K. Dewangan, A. Sharma, B. Ahn. Initial hydrogenation in multiphase TiFeCoNiCu high-entropy alloy for hydrogen storage. Journal of Alloys and Compounds 1022, 179711 (2025) .

17 J. W. Yeh, S. K. Chen, S. J. Lin, J. Y. Gan, T. S. Chin, T. T. Shun, C. H. Tsau, S. Y. Chang. Nanostructured high-entropy alloys with multiple principal elements: novel alloy design concepts and outcomes. Advanced Engineering Materials 6, 299–303 (2004).

18 S. Guo, C. Ng, J. Lu, C. T. Liu. Effect of valence electron concentration on stability of fcc or bcc phase in high entropy alloys. Journal of Applied Physics 109, 103505 (2011).

19 S. Guo, Q. Hu, C. Ng, C. T. Liu. More than entropy in high-entropy alloys: forming solid solutions or amorphous phase. Intermetallics 41, 96–103 (2013).

20 M. C. Oh, A. Sharma, H. Lee, B. Ahn. Phase separation and mechanical behavior of AlCoCrFeNi-X (X = Cu, Mn, Ti) high entropy alloys processed via powder metallurgy. Intermetallics 139, 107369 (2021).

21 H. Lee, A. Sharma, M. Kim, B. Ahn. Correlation between the nanomechanical characteristic and the phase transformation of BCC-based high entropy alloys produced via powder metallurgy. Powder Metallurgy 66, 669–678 (2023).

22 R. Silva, R. L. Lean Neto, D. R. Leiva, T. T. Ishikawa, C. S. Kiminami, A. M. Jorge Jr., W. J. Botta. Room temperature hydrogen absorption by Mg and Mg TiFe nanocomposites processed by high-energy ball milling. International Journal of Hydrogen Energy 43, 12251–12259 (2018).

23 C. Suryanarayana. Mechanical alloying and milling. Progress in Materials Science 46, 1–184 (2001) .

24 A. S. Rogachev, S. G. Vadchenko, N. A. Kochetov, S. Rouvimov, D. Yu. Kovalev, A. S. Shchukin, D. O. Moskovskikh, A. A. Nepapushev, A. S. Mukasyan. Structure and properties of equiatomic CoCrFeNiMn alloy fabricated by high-energy ball milling and spark plasma sintering. Journal of Alloys and Compounds 805, 1237–1245 (2019).

25 A. Kumar, N. K. Mukhopadhyay, T. P. Yadav. Hydrogen storage in high entropy alloys. International Journal of Hydrogen Energy 47, 11236–11249 (2022).

26 M. M. Nygård, G. Ek, D. Karlsson, M. Sahlberg, M. H. Sørby, B. C. Hauback. Counting electrons – a new approach to tailor the hydrogen sorption properties of high-entropy alloys. Acta Materialia 175, 121–129 (2019).

27 M. Naderloo, H. Hajibeygi, A. Pluymakers. Hydrogen solution exposure at a seasonal timescale does not affect the geomechanical properties of clay-rich sandstones. Scientific Reports 15, 35908 (2025).

28 J. Murray, H. Miller, P. Bird, A. J. Goudy. The effect of particle size and surface composition on the reaction rates of some hydrogen storage alloys. Journal of Alloys and Compounds 231, 841–845 (1995).

29 M. Hirscher, B. Panella. Nanostructures with high surface area for hydrogen storage. Journal of Alloys and Compounds 404–406, 399–401 (2005).

30 F. Yang, J. Wang, Y. Zhang, Y. Zhang, Z. Wu, Z. Zhang, F. Zhao, J. Huot, J. G. Novaković, N. Novaković. Recent progress on the development of high entropy alloys (HEAs) for solid hydrogen storage: a review. International Journal of Hydrogen Energy 47, 11236–11249 (2022).

31 E. M. Dematteis, N. Berti, F. Cuevas, M. Latroche, M. Baricco. Substitutional effects in TiFe for hydrogen storage: a comprehensive review. Materials Advances 2, 2524–2560 (2021).